THE JOURNAL OF PHYSICAL CHEMISTRY B

Article

Cite This: J. Phys. Chem. B XXXX, XXX, XXX−XXX

pubs.acs.org/JPCB

Dynamics of Dicyanamide in Ionic Liquids is Dominated by Local Interactions

Johannes Hunger,*[,†] Soham Roy,[†,‡] Maksim Grechko,[†] and Mischa Bonn[†]

[†]Max Planck Institute for Polymer Research, Ackermannweg 10, 55128 Mainz, Germany

[‡]Graduate School Materials Science in Mainz, Staudingerweg 9, 55128 Mainz, Germany

Supporting Information

ABSTRACT: The dynamics of probe molecules is commonly used to investigate the structural dynamics of room-temperature ionic liquids; however, the extent to which this dynamics reflects the dynamics of the ionic liquids or is probe specific has remained debated. Here, we explore to what extent the vibrational and rotational dynamics of the dicyanamide anion, a common ionic liquid anion, correlates with the structural relaxation of ionic liquids. We use polarization-resolved, ultrafast infrared spectroscopy to probe the temperature- and probe-concentration-dependent dynamics of samples with small amounts of 1-ethyl-3-methylimidazolium ($[emim]^+$) dicyanamide ($[DCA]^-$) dissolved in four $[emim]^+$-based ionic liquids with tetrafluoroborate ($[BF_4]^-$), bis(trifluoromethylsulfonyl)-imide ($[NTf_2]^-$), ethylsulfate ($[EtSO_4]^-$), and triflate ($[OTf]^-$) as anions. The transient spectra after broad-band excitation at 2000−2300 cm^{-1}, resonant with the symmetric and antisymmetric C≡N stretching vibrations, initially contain oscillatory signatures due to the vibrational coherence between both modes. Vibrational population relaxation occurs on two distinct time scales, ∼6−7 and ∼15−20 ps. The vibrational dynamics is rather insensitive to the details of the ionic liquid anion and temperature, except for the slow vibrational relaxation component. The decay of the excitation anisotropy, a measure of the rotational dynamics of $[DCA]^-$, markedly depends on temperature, and the obtained decay time exhibits an activation energy of ∼15−21 kJ/mol. Remarkably, neither the rotation time nor the activation energy can be simply explained by the variation of the macroscopic viscosity. Hence, our results suggest that the dynamics of dicyanamide is only in part representative of the ionic liquid structural dynamics. Rather, the dynamics of the probe anion seems to be determined by the specific interaction of $[DCA]^-$ with the ionic liquid's ions for the class of $[emim]^+$-based ionic liquids studied here.

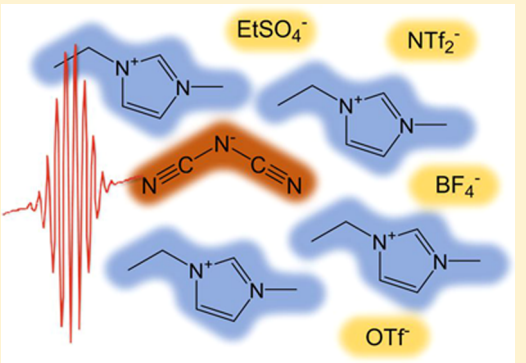

INTRODUCTION

The dynamics of room-temperature ionic liquids (RTILs) has been intensively studied using various experimental and computational methods over the last few decades.[1−9] This dynamics is closely related to the rich structural motifs of ionic liquids[10,11] and also critically affects the kinetics of reactions when using RTILs as reaction media.[12] As the dynamics of the ions constituting the ionic liquids can rarely be probed directly,[13−16] most comprehensive information has been obtained using probe molecules that can be investigated with visible light:[5,17−21] the rotational dynamics of fluorescent dyes as probe molecules and also the solvation response of the ionic liquid can be readily observed over time scales ranging from femtoseconds to nanoseconds. From these studies, it has become apparent that the solvation response of ionic liquids is rather complex, occurs on multiple time scales, and differs from that of conventional molecular solvents.[5] There has, however, also been evidence that the experimentally determined solvation response markedly depends on the chemical nature of the dye used as a molecular probe.[6,17,22] Moreover, not only the specific interaction of the dye with the ionic liquid but also the bare geometry (size) of the molecule affects the measured dynamics.[1] Although the use of relatively large dyes provided valuable insight into the solvation of large solutes in ionic liquids, the solvation dynamics on smaller length scales could not be resolved.[1]

To study the solvation of molecules and ions with sizes comparable to those of the ionic liquids' ions, ultrafast infrared spectroscopies have become popular in recent years.[8,16,23−30] Among these studies, small anions with prominent vibrational signatures[31] like SCN^-,[8,26−28,30] $SeCN^-$,[32] and N_3^-[25−27,29] have emerged as powerful vibrational probes. Using such anionic probe molecules, the vibrational relaxations of the C≡N and N≡N stretching vibrations have been used to obtain information on their coupling to the ionic liquid environment;[25,27] their rotational dynamics has been used to infer information on hydrodynamic friction;[8,32] and the temporal evolution of the vibrational frequencies (frequency−frequency correlations) has made structural (solvation cage) fluctuations in ionic liquids experimentally accessi-

Received: November 7, 2018
Revised: February 4, 2019
Published: February 5, 2019

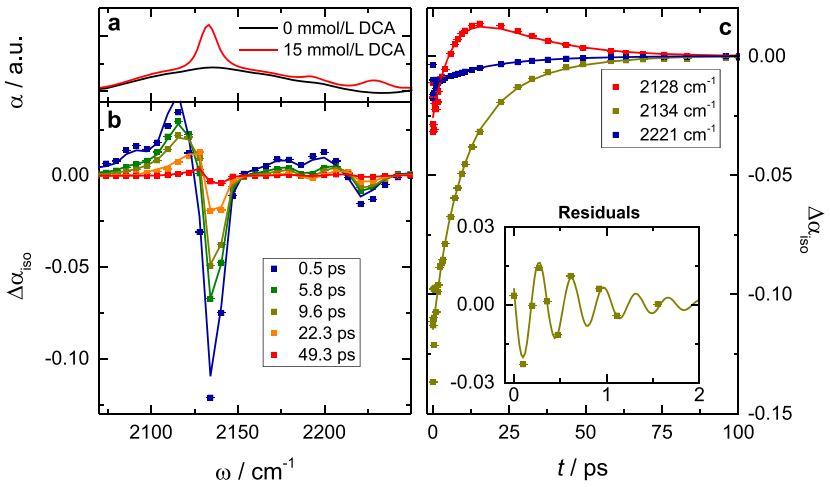

Figure 1. (a) Linear infrared absorption spectrum of [emim][BF_4] containing 0 (solid black line) and 15 mmol/L (solid red line) [emim][DCA]. (b) Transient isotropic absorption spectra, $\Delta\alpha_{iso}$, for 15 mmol/L [emim][DCA] in [emim][BF_4] at 22 °C at different delay times after broad-band infrared excitation. (c) Transient isotropic signals at representative probe frequencies as a function of delay time, *t*. Symbols in panels (b) and (c) show experimental data; error bars show standard deviation on a pulse-to-pulse basis; and solid lines correspond to fits using the kinetic model (see the text). The inset in panel (c) shows the residuals (symbols) of fitting the kinetic model at 2134 cm^{-1} to the experimental data at short delay times. The solid line shows a damped oscillation with a 350 fs (95 cm^{-1}) oscillation period.

ble.[29,30,33] From these pioneering studies, it has become apparent that fluctuations and friction scale with macroscopic dynamical properties like the RTIL's viscosity upon variation of the cation, thus suggesting that the used anionic vibrational probes directly investigate ionic liquid dynamics.[8,32] However, it has also been shown that the counterion of the anionic vibrational probe affects the measured dynamics as K^+ cations tend to induce clustering of the vibrational probe anions.[32,33]

Here, we explore the use of dicyanamide {$[DCA]^-$, $N(CN)_2^-$} as a vibrational probe.[27] $[DCA]^-$ is, in fact, a widely used anion in ionic liquids, and DCA-based ionic liquids feature low viscosities.[34] To use $[DCA]^-$ as a vibrational probe, we dissolve small amounts (≤75 mmol/L) of [emim][DCA] in $[emim]^+$-based ionic liquids. With polarization-resolved infrared pump−probe spectroscopy, we excite the C≡N stretching vibrations of $[DCA]^-$ and monitor the temporal and angular evolutions of the excited vibrational modes. From these experiments, we extract the vibrational population dynamics and the rotational dynamics of the $[DCA]^-$ anion in different ionic liquids. To elucidate the effect of the ionic liquids' anion, we study $[DCA]^-$ in [emim][BF_4], [emim][$EtSO_4$], [emim][NTf_2], and [emim][OTf]. The thermal activation of the investigated dynamics of $[DCA]^-$ is extracted from temperature-dependent experiments at temperatures ranging from 22 to 85 °C.

EXPERIMENTAL SECTION

Materials. All ionic liquids used in this work, 1-ethyl-3-methylimidazolium triflate ([emim][OTf], >99%), 1-ethyl-3-methylimidazolium tetrafluoroborate ([emim][BF_4], >99%), 1-ethyl-3-methylimidazolium ethyl sulfate ([emim][$EtSO_4$] >99%), 1-ethyl-3-methylimidazolium dicyanamide ([emim][DCA], >98%), and 1-ethyl-3-methylimidazolium bis(trifluoromethylsulfonyl)imide ([emim][NTf_2], >99%), were purchased from IoLiTec, Ionic Liquids Technologies GmbH (Germany). Ionic liquids were dried in vacuo for >2 days. Samples were prepared gravimetrically by weighing the appropriate amount of ionic liquids into a sample vial using an analytical balance. We prepared samples containing 15, 30, 45, 60, and 75 mmol/L [emim][DCA] in [emim][BF_4]. For all other ionic liquids ([emim][OTf], [emim][$EtSO_4$], and [emim][NTf_2]), we studied samples containing 45 mmol/L [emim][DCA]. To avoid water uptake, all samples were stored over molecular sieves (4 Å). To remove any solid residuals from the molecular sieves, samples were centrifuged prior to the experiments. For all infrared spectroscopy experiments, the samples were contained between CaF_2 windows separated by a ~25 μm PTFE spacer. For temperature-dependent experiments, the sample cell is mounted in a temperature-controlled sample holder,[15] which can be heated by four cartridge heater elements powered by a remotely controlled Voltcraft PPS 36 V power supply. The temperature of the sample is probed using a PT100 temperature sensor mounted in the housing close to the sample cell. Temperature is controlled to an accuracy of ±1 °C using a Fuji PXG4 Fuzzy Logic PID controller.

Polarization-Resolved Femtosecond Infrared Spectroscopy. The femtosecond infrared experiments[15,35,36] are based on mid-infrared pulses with a pulse duration of ~80 fs and a pulse energy of ~14 μJ centered at ~2150 cm^{-1} (full width at half-maximum of ~300 cm^{-1}). These infrared pulses were generated from 800 nm (1 kHz repetition rate) pulses obtained from a commercial Ti:sapphire regenerative amplifier (Spitfire Ace, Spectra-Physics). A total of 1.5 mJ of these 800 nm pulses is used to pump a commercial, double-stage optical parametric amplifier, OPA, (TOPAS prime, Light Conversion). In a subsequent difference frequency mixing stage, the signal and idler pulses are mixed in a GaSe crystal yielding the mid-infrared pulses. The residual signal and idler pulses are split off using two CaF_2-based dichroic mirrors and a silicon-based long-wave-pass filter.

A wedged CaF_2 window is used to split off two small fractions of the infrared light (~4% each). The front reflection of the wedged window is used as a probe beam, whereas the back reflection serves as a reference beam. The transmitted mid-IR beam (~90%) is used as the pump beam. The pump beam is modulated at 500 Hz using a mechanical chopper and directed on a translational stage to control the timing (delay time, *t*) relative to the probe beam. The polarization of the

DOI: 10.1021/acs.jpcb.8b10849
J. Phys. Chem. B XXXX, XXX, XXX−XXX

pump beam is rotated to 45° relative to the probe beam using an achromatic $\lambda/2$ wave plate. The pump and the probe beams are focused into the sample using an off-axis parabolic mirror. After transmission through the sample, the pump beam is blocked and the probe beam is re-collimated using a second parabolic mirror. A wire-grid polarizer mounted on a motorized rotation stage allows selecting the polarization components of the probe beam parallel or perpendicular to the pump-pulse polarization. The probe and the reference beams are focused onto the slit of an imaging spectrograph (Triax 180, Horiba Scientific), which spectrally disperses both beams onto a liquid-nitrogen-cooled 2 × 32 pixel mercury cadmium telluride detector to record the frequency-dependent intensity of the probe and the reference beams. The pump-induced modulation of the sample is obtained as a function of infrared frequency, ω, by recording the ratio of the transmitted probe intensities in the presence (I) and absence (I_0) of the pump beam. This ratio was normalized by the intensities of the reference beam, I_R and $I_{R,0}$, to correct for pulse-to-pulse fluctuations in the probe intensity. The transient absorption spectra parallel $[\Delta\alpha_{\parallel}(\omega, t) = -\ln(I_{\parallel}/I_{\parallel,0}\cdot I_{R,0}/I_R)]$ and perpendicular $[\Delta\alpha_{\perp}(\omega, t) = -\ln(I_{\perp}/I_{\perp,0}\cdot I_{R,0}/I_R)]$ to the pump polarization are obtained from the transmitted intensities and used to construct the isotropic transient signal[36]

$$\Delta\alpha_{iso}(\omega, t) = \frac{\Delta\alpha_{II}(\omega, t) + 2\Delta\alpha_{\perp}(\omega, t)}{3} \quad (1)$$

which contains the vibrational population dynamics and subsequent thermal dynamics but is independent of orientational dynamics.

Because of its linear polarization, the pump pulse preferentially excites molecules with transition dipole moment parallel to the pump polarization. Thus, the excitation is anisotropic, and we quantify the anisotropy via the anisotropy parameter, $R(\omega, t)$[35−37]

$$R(\omega, t) = \frac{\Delta\alpha_{II}(\omega, t) - \Delta\alpha_{\perp}(\omega, t)}{\Delta\alpha_{II}(\omega, t) + 2\Delta\alpha_{\perp}(\omega, t)} \quad (2)$$

As molecular reorientation and/or energy transfer scrambles the preferential orientational distribution of the excited oscillators, $R(\omega, t)$ approaches 0.[36]

RESULTS AND DISCUSSION

Infrared Absorption Spectra. In Figure 1a, we show the infrared absorption spectra of a sample of [emim][BF_4] together with [emim][BF_4] containing 15 mmol/L [emim]-[DCA]. Addition of small amounts of dicyanamide to [emim][BF_4] results in the emergence of three distinct vibrational bands in the ω = 2100−2250 cm^{-1} range. The most intense band due to $[DCA]^-$ is centered at 2130 cm^{-1} and has been assigned to the antisymmetric C≡N stretching vibration of $[DCA]^-$.[27] We also observe two weaker vibrational modes at 2190 and 2230 cm^{-1}. These two bands have been attributed to the symmetric C≡N stretching vibrations and a combination band of the symmetric C−N and antisymmetric C−N stretching modes. In contrast to previous work,[27] we, however, arrive at the reverse assignment of these two modes: we attribute the weak feature at ∼2190 cm^{-1} to the combination of the asymmetric C−N stretching vibration at 900 cm^{-1} and the symmetric C−N stretching vibration at 1300 cm^{-1} (see Supporting Information (SI), Figure S1). The vibrational mode at 2230 cm^{-1} we assign to the symmetric C≡N stretching band. A Fermi resonance between these two modes can explain the relatively high absorption cross section of the, in principle forbidden, vibrational transition of the combination mode and also the slight red shift of the combination band relative to the sum of the two fundamental C−N vibrational frequencies (observed frequency 2190 cm^{-1} vs combination frequency 900 + 1300 cm^{-1}).

Isotropic Vibrational Dynamics. In the femtosecond infrared experiments, we use a broad-band infrared excitation pulse centered at ∼2150 cm^{-1}, resonant with all three vibrational modes of the $[DCA]^-$ anion described above. At short delay times, the transient isotropic vibrational spectra (see Figure 1b, t = 0.5 ps) show a pump-induced bleach at the fundamental frequency of the antisymmetric stretching band, 2130 cm^{-1}. This bleach indicates the population of the v = 1 vibrational excited state and depletion of the vibrational ground state of this mode. The adjacent induced absorption at ∼2110 cm^{-1} originates from the excited-state absorption (v = 2 ← 1). Remarkably, the spectral shape of the induced absorption depends on t: at an early delay, the maximum of the induced absorption is located at ∼2115 cm^{-1} and this maximum gradually shifts to ∼2125 cm^{-1} with increasing t. At early times (t < 10 ps), we also observe a shoulder at ∼2090 cm^{-1}, which is absent at later delay times. Together, the spectral changes of the induced absorption as a function of time point toward a change of the populated vibrational states in the course of energy relaxation (see also the discussion of the kinetic model below). Similar but weaker spectral features at 2220 cm^{-1} ($\Delta\alpha_{iso}$ < 0) and 2200 cm^{-1} ($\Delta\alpha_{iso}$ > 0) provide evidence for the population of the excited state of the symmetric C≡N stretching band. Both transient spectral signatures decay with increasing delay time due to vibrational relaxation and dissipation of the excess vibrational energy. We observe at all delay times a slight dip in the transient spectra at 2190 cm^{-1}, which may result from the population of the combination band and/or coupling of C≡N stretching modes to the combination band.

The decays of $\Delta\alpha_{iso}$ at the center of the bleach signal for the symmetric (2221 cm^{-1}) and antisymmetric (2134 cm^{-1}) C≡N stretch bands are displayed in Figure 1c. As can be seen from this figure, the transient signals decay to 0 within 100 ps. Notably, the transient signal at 2128 cm^{-1} (Figure 1c) is negative (bleach) at t < 5 ps and becomes positive (induced absorption) at t > 5 ps. This change shows that the transient signals decay with at least two different relaxation times (i.e., a short-lived transient signal with a negative transient signature and a longer-lived signal with a positive transient spectral component at this frequency).

To quantify the vibrational relaxation dynamics and the associated vibrational spectra, we fit a kinetic model[38] to the experimental $\Delta\alpha_{iso}(\omega, t)$ data. As mentioned above, at least two disparate relaxation times are needed to describe the data. Thus, we have tested different relaxation models with up to four relaxation times to model the $\Delta\alpha_{iso}(\omega, t)$ data. However, models with more than two relaxation times, which would, for instance, account for the energy transfer between the symmetric and antisymmetric C≡N stretching modes and relaxation, provided scattered relaxation times at different concentrations of $[DCA]^-$ and thus did not provide a consistent relaxation model. As such, energy exchange between the stretching modes, which would be readily accessible from two-dimensional (2D) IR experiments, cannot be resolved on the basis of our pump−probe experiments and is thus either

DOI: 10.1021/acs.jpcb.8b10849
J. Phys. Chem. B XXXX, XXX, XXX−XXX

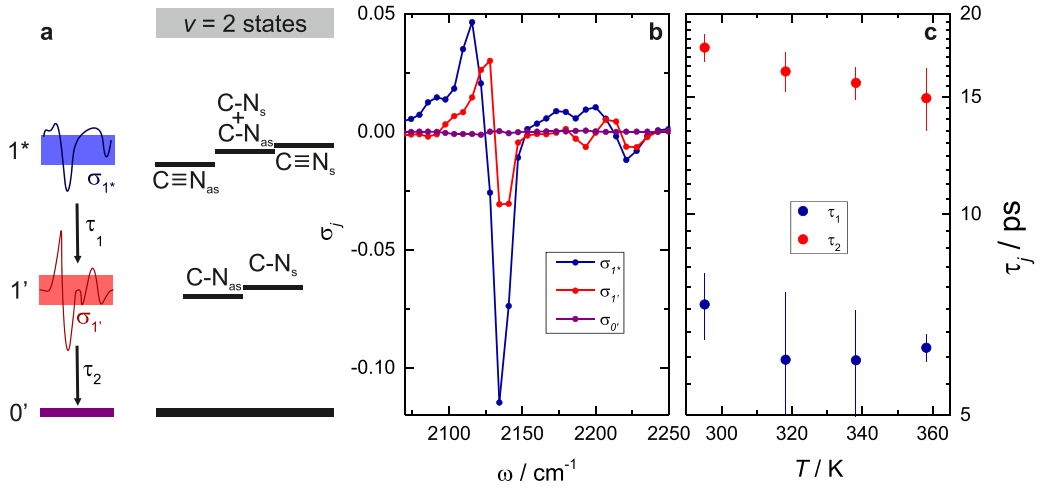

Figure 2. (a) Schematic representation of the kinetic model (left), in which the excited state 1* decays to the intermediate state 1′, which eventually relaxes to the heated ground state 0′. Also shown are the possible vibrational states (right) that may contribute to the modeled populations (C−N and C≡N stretching modes; subscripts refer to symmetric (s) and antisymmetric (as) stretching modes). (b) Associated transient spectra of the excited state σ_{1*}, the intermediate state $\sigma_{1'}$, and the heated ground state $\sigma_{0'}$, as extracted from fitting the kinetic model (see the text) to the $\Delta\alpha_{iso}(\omega, t)$ data for 15 mmol/L [emim][DCA] in [emim][BF_4] at 22 °C. (c) Relaxation times τ_1 and τ_2 for [emim][DCA] in [emim][BF_4] as a function of temperature, T. Symbols correspond to the average values obtained from different concentrations of [emim][DCA] (15, 30, 45, 60, and 75 mmol/L), and the error bars represent the corresponding standard deviation.

insignificant or too rapid to resolve, thereby reaching a steady state: we find that two relaxation times suffice to describe our experimental data. A kinetic model based on two relaxation times can be implemented using (i) a parallel model with two distinct excited states relaxing independently with disparate relaxation times to a common ground state or (ii) a cascading model where an excited state transiently populates an intermediate state, which subsequently relaxes to the ground state. For the present experiments with the symmetric and antisymmetric C≡N stretching modes dominating the transient signals, both models are conceivable. Unfortunately, both scenarios cannot be discriminated on the basis of the $\Delta\alpha_{iso}(\omega, t)$ data as they describe the data equally well, yet with different associated transient spectra and different physical meanings. For the present data, independent excitation and relaxation of the symmetric and antisymmetric stretching vibrations with two relaxation times [model (i)] yielded spectra associated with both excited states that are inconsistent with independent relaxation of both states (see Figure S2, SI). Hence, we use in the following analysis a cascading model with two consecutive relaxation rates (ii): the initially excited state 1* transiently populates an intermediate state 1′ with a relaxation time τ_1. The intermediate state 1′ subsequently relaxes with τ_2 to a (heated) ground state 0′ (see Figure 2a). Note that due to the dissipation of the excess vibrational energy and the resulting increase of the sample temperature, the heated ground state may differ from the ground state prior to excitation: due to thermally induced shifts of vibrational modes, the observed transient signals at long times may still be finite ($\Delta\alpha_{iso} \neq 0$).

Assuming the same vibrational dynamics at all probe frequencies, this model excellently describes the transient isotropic data over the entire frequency and delay time ranges (solid lines in Figure 1b,c). Only at $t < 2$ ps, we find marked deviations of the data from the fit with well-defined oscillations of the residuals as a function of delay time (see the inset of Figure 1c). The residuals can be well described by a damped harmonic oscillation (oscillation period of 350 fs, corresponding to a frequency of 95 cm^{-1}; see the solid line in the inset of Figure 1c). This oscillation originates from the vibrational coherence[39,40] between the antisymmetric and symmetric C≡N stretching vibrations, which leads to a regular oscillation at the difference frequency of both bands (2230−2130 ≈ 95 cm^{-1}). The coherence, however, rapidly de-phases with a coherence decay time of 0.77 ps and thus hardly contributes at delay times beyond 2 ps. The rapid de-phasing is indicative of a weak correlation of the frequency fluctuations of the symmetric and antisymmetric modes.

From fitting the kinetic model (Figure 2a) to the experimental data, we obtain the associated transient spectra of these states, σ_j (j = 1*, 1′, and 0′). The thus-obtained spectra (Figure 2b) have transient signals at frequencies characteristic for both the antisymmetric and the symmetric stretching modes. The modulation of the vibrational response across the entire studied spectral range may stem from excited-state populations of the symmetric and antisymmetric stretching vibrations contributing to the transient signals. However, anharmonic coupling (see above) and possibly vibrational energy transfer between both vibrations also can modulate the vibrational response at all probe frequencies, independent of the identity of the excited vibration. Indeed, σ_{1*} shows a strong modulation of the antisymmetric stretching band with a bleach at ∼2130 cm^{-1} and red-shifted induced absorption and similar features at ∼2220 and ∼2180 cm^{-1} for the symmetric stretching band. Both excited-state absorptions exhibit a double-peak structure at 2080−2125 and 2150−2210 cm^{-1} for the antisymmetric and symmetric modes, respectively. These double peaks are likely due to the rather complex vibrational structure of the ν = 2 vibrational states (see also Figure 2a): the double-peak structure indicates at least two distinct transitions from the ν = 1 states. The contribution of these signatures of 1* to the measured $\Delta\alpha_{iso}(\omega, t)$ data decay with a time constant of $\tau_1 \approx 7$ ps at ambient temperature.

The extracted spectra of the intermediate state, $\sigma_{1'}$ comprise three bleaching signals at the frequencies of the antisymmetric stretch band, the combination band, and the symmetric stretch

DOI: 10.1021/acs.jpcb.8b10849
J. Phys. Chem. B XXXX, XXX, XXX−XXX

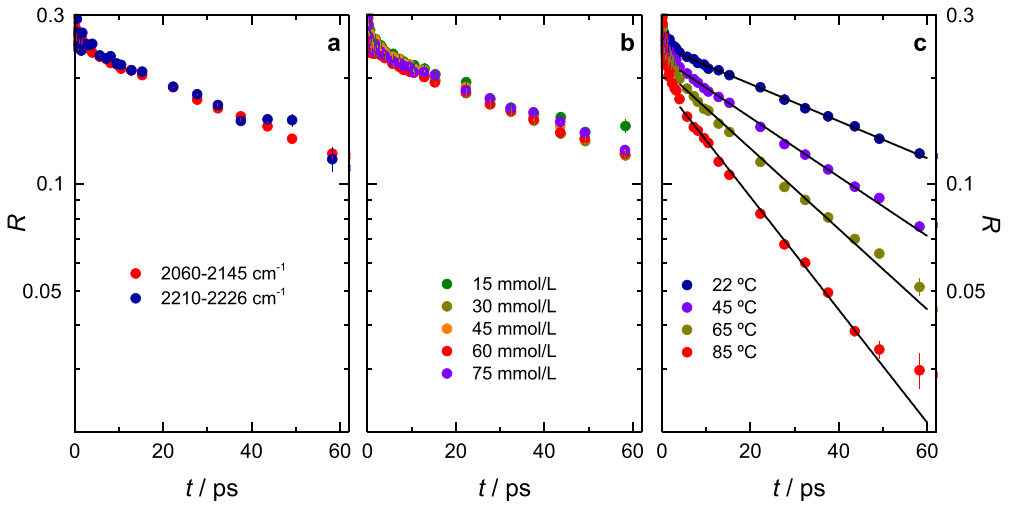

Figure 3. (a) Excitation anisotropy, R, averaged over frequencies characteristic for the antisymmetric C≡N stretching vibration (red symbols) and for the symmetric C≡N stretching mode (blue symbols) for 45 mmol/L [emim][DCA] in [emim][BF_4] at 22 °C. (b) $R(t)$ decays for different concentrations of [emim][DCA] in [emim][BF_4] at 22 °C. (c) $R(t)$ decays for 45 mmol/L [emim][DCA] in [emim][BF_4] for different temperatures. Symbols in all panels correspond to the experimental values, and error bars correspond to the experimentally obtained standard deviation. Solid lines in panel (c) show the fits of a single exponential decay to the experimental data at delay times ranging from 4 to 60 ps.

band, together with induced absorptions at ∼2100 and ∼2200 cm^{-1} (Figure 2b). The most apparent differences between the spectra of 1* and 1′ at frequencies of the antisymmetric C≡N stretch mode are the absence of the shoulder at ∼2090 cm^{-1} in the $\sigma_{1'}$ spectrum and the blue shift of the maximum of the induced absorption of $\sigma_{1'}$ as compared to σ_{1*}. With these features, our model can explain, through the relaxation from 1* to 1′, both the disappearance of the double-peak structure of the induced absorption with time and the blue shift of the positive features at ∼2120 cm^{-1} with increasing t. Relaxation to the state 1′ depopulates the state 1* and, thus, eliminates transitions to the $v = 2$ states (Figure 2a). Instead of transitions to the manifold of the second excited states, the transient signal is due to the coupling between the states of 1′ and the C≡N stretching modes, which results, among others, in a blue shift of the transient induced absorption related to the antisymmetric C≡N stretching band. Given that the combination band of the C−N stretching bands is nearly resonant with the C≡N stretching modes, we hypothesize that the intermediate state 1′ of the model involves a population of the C−N stretching modes (Figure 2a). At ambient temperature, the contribution of 1′ to the transient signals relaxes with $\tau_2 \approx 18$ ps to the thermal state 0′ with its transient spectrum $\sigma_{0'}$ nearly 0 at all probe frequencies (Figure 2b). Thus, dissipation of the vibrational energy into a thermally accessible state does not result in a significant change of the vibrational response of $[DCA]^-$.

We note that both τ_1 and τ_2 somewhat differ from the values reported for $[DCA]^-$ in 1-butyl-3-methylimidazolium tetrafluoroborate (8.5 ps)[27] and $[DCA]^-$ in 1-butyl-2,3-dimethylimidazolium tetrafluoroborate (11 ps).[27] In addition to the different RTIL cations of these studies,[27] the reported relaxation times were obtained using a monoexponential relaxation at detection frequencies centered at the antisymmetric stretching mode. As such, the literature values may represent the amplitude-weighted average of the τ_1 and τ_2 values reported here. Moreover, the experiments of Dahl et al.[27] were based on narrower excitation pulses (∼150 cm^{-1}), which were tuned to be resonant with the combination band and the symmetric stretching mode. In this work, the infrared pulses are resonant with all $[DCA]^-$ modes described above. As such, the energy transfer between the modes may lead to longer τ_2 values as compared to those in the literature.[27]

From our experimental results, we find the isotropic vibrational relaxation times τ_j and the associated spectra σ_j for [emim][DCA] in [emim][BF_4] to be virtually independent of the concentration of $[DCA]^-$ within the range of 15−75 mmol/L $[DCA]^-$. Upon variation of temperature, we find a minor decrease of τ_2 from 18 ps at 22 °C to ∼15 ps at 85 °C (Figure 2c). The temperature dependence of τ_1 is less pronounced. Also, variation of the anion (experiments of 45 mmol/L [emim][DCA] in [emim][OTf], [emim][NTf_2], and [emim][$EtSO_4$]) yields very similar results for the isotropic dynamics (see Figure S3, SI) as a function of temperature. Notably, we find τ_2 to vary with the nature of the anion: $\tau_2 \approx$ 19.9 ps for $[DCA]^-$ in [emim][$EtSO_4$], $\tau_2 \approx 16.2$ ps for $[DCA]^-$ in [emim][NTf_2], and $\tau_2 \approx 18.6$ ps for $[DCA]^-$ in [emim][OTf] at 22 °C (see Figure S3, SI). This trend in vibrational relaxation times, τ_2, loosely correlates with the viscosities of the ionic liquids ([emim][BF_4]: 36 mPa s,[41] [emim][$EtSO_4$]: 98 mPa s,[42] [emim][NTf_2]: 32 mPa s,[43] and [emim][OTf]: 43 mPa s[44] at 25 °C). Similar to the dependence of τ_2 on the RTIL anion, its temperature dependence shows a decrease of τ_2 with decreasing viscosity (increasing T, see Figure S4 in the SI for the correlation between viscosity and τ_2). As vibrational energy relaxation goes along with the transfer of the energy to lower energy modes in the molecule and/or the surrounding bath, the dynamics depends on the energy of the excited mode, the accepting mode(s), and on the coupling between these modes. The overall correlation between τ_2 and the viscosity of the ionic liquids suggests that the RTIL dynamics imposes fluctuations (of coupling strengths or frequency) on the modes relevant to the vibrational relaxation. The correlation can be explained by these fluctuations constituting the rate-limiting step in a relaxation pathway.

Rotational Dynamics via Excitation Anisotropy. For the presently studied systems, the transient signals retain their

DOI: 10.1021/acs.jpcb.8b10849
J. Phys. Chem. B XXXX, XXX, XXX−XXX

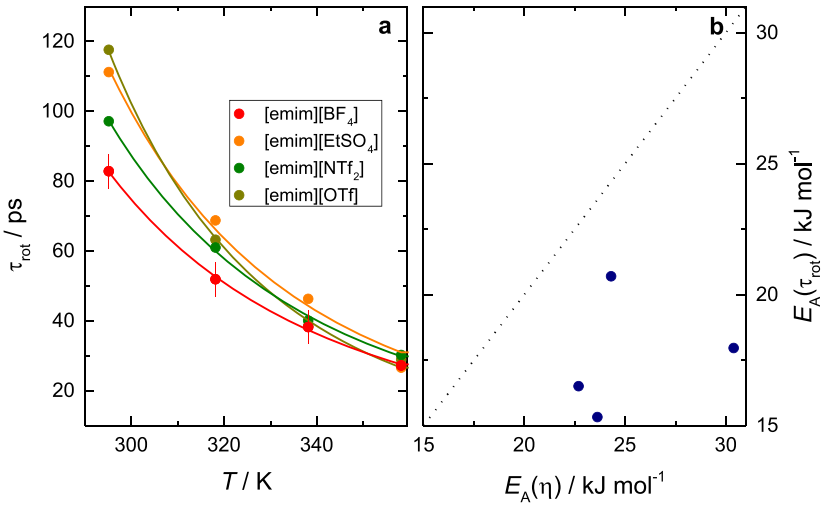

Figure 4. (a) Rotational correlation time, τ_{rot}, as obtained from fitting a monoexponential decay to the $R(t)$ decays averaged at 2060−2145 cm^{-1} for the different RTILs as a function of temperature, T. Symbols show the values of τ_{rot} obtained from the monoexponential fits. Error bars are exemplarily shown for [emim][BF_4] and correspond to the standard deviation within experiments using 15, 30, 45, 60, and 75 mmol/L [emim][DCA] in [emim][BF_4]. The solid lines correspond to fits using an Arrhenius-type thermal activation. (b) Activation energy for τ_{rot}, [$E_A(\tau_{rot})$], obtained from fitting an Arrhenius equation to the data in panel (a) as a function of the corresponding activation energy for the viscosity $E_A(\eta)$ of the samples. $E_A(\eta)$ values were obtained by fitting an Arrhenius equation to viscosities reported in the literature[41−44] at temperatures ranging from 293 to 360 K.

anisotropy, $R(t)$, which is a measure of the orientational memory of the $[DCA]^-$ on the excitation polarization, for delay times as long as 60 ps (see Figure 3). In general, excitation of randomly distributed, uncoupled oscillators is expected to result in an initial value of $R(t = 0) \approx 0.4$.[35] This initial value results from the excitation probability depending on the (squared) component of the transition dipole moment of the infrared-active mode along the pump-pulse polarization for isotropically distributed transition dipoles. For all samples of the present study, we find the value of $R(t = 0) < 0.4$ (Figure 3). This lower value can be explained by the simultaneous excitation of both symmetric and antisymmetric C≡N modes since they are coupled (see above, the inset of Figure 1c): for a given molecular orientation, the excitation probabilities for both $[DCA]^-$ modes differ as a result of the different orientations of the transition dipoles of these two normal modes within the molecule. Anharmonic coupling will modulate all probe frequencies and thus reduce the initial value of the excitation anisotropy. In other words, in the present pump−probe experiment, we detect the sum of both the diagonal and the off-diagonal spectral features of a 2D IR experiment, which have distinctively different polarization dependence and thus the initial value of R may be reduced. Additionally, fast energy transfer between both modes may additionally reduce $R(t = 0)$.

With increasing t, simultaneous excitation of both modes and subsequent intramolecular vibrational energy transfer between the two modes with differently aligned transition dipoles may constitute an additional decay channel for the excitation anisotropy.[45] As energy transfer rates between the two vibrations are inherently asymmetric and transfer from higher (lower) energy modes to lower (higher) energy modes is faster (slower) due to the necessary release (uptake) of energy to (from) the bath, the different transfer rates would lead to frequency-dependent $R(t)$ decays. Similarly, relaxation from the symmetric (antisymmetric) C≡N stretching band to the intermediate state 1′ could lead to a frequency-dependent decay of $R(t)$: given that the peak amplitudes (transition dipoles) of the symmetric and antisymmetric stretching vibrations (Figure 1a) are very different, the excitation probabilities of both modes are different. Thus, the population of the 1′ state generated by relaxation from the symmetric and antisymmetric modes would be significantly different and result in the different $R(t)$ decays around ∼2220 and ∼2130 cm^{-1} because of the coupling between the 1′ and both C≡N stretching modes. To assess the potential contribution of excitation of both C≡N stretching modes to $R(t)$, we compare the $R(t)$ decays averaged over probe frequencies characteristic for the antisymmetric C≡N stretching mode (2060−2145 cm^{-1}) and for the symmetric C≡N stretching mode (2210−2226 cm^{-1}). As can be seen from Figure 3a, after an initial rapid decay of $R(t)$ at short delay times, where also oscillations due to the vibrational coherence significantly contribute, the anisotropies detected in both probe frequency ranges virtually overlap. Hence, we conclude that excitation of both C≡N stretching modes does not result in additional decay mechanisms of $R(t)$ at $t > 2$ ps.

Another possible mechanism for the decay of the excitation anisotropy is intermolecular energy transfer that leads to the modulation of the vibrational response of initially not excited $[DCA]^-$ anions: energy transfer between excited and non-excited C≡N stretching modes of different molecules (with different molecular alignments)[45,46] and/or energy transfer to lower energy modes (e.g., heating of the sample), which can modulate the vibrational response of the probed vibrations,[14,36,47] result in a decay of $R(t)$. Importantly, both these intermolecular transfer mechanisms depend on intermolecular distances and thus depend on the volume concentration of the probe oscillators. As apparent from Figure 3b, the experimentally determined $R(t)$ decays for [emim][DCA] in [emim][BF_4] at 22 °C are virtually independent of the concentration of $[DCA]^-$ within the investigated concentration range (15−75 mmol/L). Hence, our data indicate that intermolecular energy transport does not contribute to the measured $R(t)$ decays. Additionally, the absence of the concentration dependence of the $R(t)$ decays

DOI: 10.1021/acs.jpcb.8b10849
J. Phys. Chem. B XXXX, XXX, XXX−XXX

suggests that the contribution of delocalized modes due to aggregation and coupling of $[DCA]^-$ anions is insignificant, in line with the nearly ideal mixing of [emim][DCA] and $[emim][BF_4]$.[48]

Given the independence of the $R(t)$ decay of the probe frequency and the $[DCA]^-$ concentration, we conclude that the main mechanism that can lead to the observed decay of $R(t > 4$ ps) is molecular rotation. Consistent with this notion, we find the decay of the anisotropy to markedly depend on temperature for 45 mmol/L $[DCA]^-$ in $[emim][BF_4]$ (Figure 3c). With increasing temperature, the excitation anisotropy decays faster, which one may expect for hydrodynamically controlled molecular rotation for which the rotation time scales with the viscosity of $[emim][BF_4]$.[8,41] We observe a similar speed-up of the $R(t)$ decays with increasing temperature for samples with 45 mmol/L $[DCA]^-$ in [emim][OTf], $[emim][NTf_2]$, and $[emim][EtSO_4]$ (see Figure S5, SI).

To quantify the decay of the anisotropy and obtain information on the rotational correlation times, we model the experimental $R(t)$ data. Since at $t < 4$ ps the vibrational coherence contributes, we restrict our analysis of the anisotropies to $t > 4$ ps. Note that using this approach, we are insensitive to any fast motion of the $[DCA]^-$ anion, such as the wobbling motion reported for $SeCN^-$ in ionic liquids.[33] As can be seen from Figures 3 and S5 (SI), a single exponential decay, $R(t) = R_0\, e^{-t/\tau}$, suffices to describe the experimental data at $4 < t/\text{ps} < 60$. The thus-obtained rotation times, τ_{rot}, (Figure 4a) vary from 83 ps ($[emim][BF_4]$) to 118 ps ([emim][OTf]) at 22 °C. Upon increasing the temperature, the extracted values of τ_{rot} decrease and we find decay times ranging from 27 ps ($[emim][EtSO_4]$) to 30 ps ($[emim][NTf_2]$) at 85 °C. The variation of τ_{rot} upon substitution of the anion is rather moderate (a factor of <1.5 at a given temperature), given that the viscosities of the RTILs differ by up to a factor of 3 ($[emim][EtSO_4]$: 98 mPa s,[42] $[emim][NTf_2]$: 32 mPa s[43] at 25 °C): also, τ_{rot} only loosely correlates with the samples viscosity (see Figure S6 in the SI), and our results thus show that the macroscopic viscosity does not solely determine the obtained values of τ_{rot}.

Similarly, the variation of τ_{rot} with temperature is decoupled from the temperature dependence of the viscosity: an Arrhenius equation, $\tau_{rot}(T) = \tau^0_{rot}\, e^{E_A/RT}$, describes the temperature dependence of the obtained τ_{rot} values well (see solid lines in Figure 4a). The obtained activation energies, $E_A(\tau_{rot}) = 15-21$ kJ/mol, are, however, systematically lower than the corresponding activation energies for the viscosity $E_A(\eta) = 23-30$ kJ/mol (see Figure 4b). Hence, we find that the energetic barrier for the rotation of $[DCA]^-$ in these ionic liquids is significantly lower than for shearing the constituting ions. In fact, such lower energetic barrier may not be too surprising because the attractive interaction between the $[DCA]^-$ anion and the RTIL ions is likely dominated by Coulombic attraction to the $[emim]^+$ cation. Since the $[emim]^+$ cation is common to all RTILs of this study, it is conceivable that the environment experienced by the $[DCA]^-$ anion is very similar for all studied RTILs. Consistent with this notion, the rotational dynamics of anionic SCN^- [8] (and also electroneutral CO_2[49]) has been shown to be very sensitive to the variation of the cation. The sensitivity of the probe dynamics to the probe molecule and its very immediate environment is also in line with what has been concluded from experiments using different azides as vibrational probes.[29] The small, yet detectable difference between the variation of τ_{rot} of $[DCA]^-$ for different anions of the RTIL in this study in turn reflects the anion dependence of the RTIL structure and the (mostly repulsive) interaction of $[DCA]^-$ with the RTIL's anions. These differences together with the dynamics of the cations, which we do not probe with our experiments, are the likely origin of the observed deviation of the RTIL dynamics of binary mixtures of [emim][DCA] and $[emim][BF_4]$ as determined from dielectric relaxation spectroscopy.[48]

CONCLUSIONS

Altogether, our results show that the vibrational dynamics of small amounts of dicyanamide in $[emim]^+$-based ionic liquids only partly reflects the overall structural dynamics of the studied RTILs. The vibrational dynamics after excitation of the C≡N stretching vibrations is rather insensitive to temperature and the nature of the RTILs, with one notable exception: after initial population and relaxation (relaxation time 6−7 ps) to intermediate state(s), the relaxation time (15−20 ps) from these intermediate state(s) depends on both temperature and the nature of the RTIL anion. This variation of the relaxation rate can be explained by frequency fluctuations that are imposed by the structural dynamics of the RTIL being part of the vibrational relaxation mechanism.

From the decay of the excitation anisotropy as a function of frequency and dicyanamide concentration, we find molecular rotation to dominate the decay mechanism. Although the reduction of the obtained rotation times with increasing temperature can in part be explained by a reduction of the viscosity, the rotation times do not simply scale with RTILs' viscosity upon substitution of the RTIL's anion. Also, the energetic barrier for the rotation of dicyanamide as determined from the temperature dependence of the anisotropy decay is markedly lower than the thermal activation barrier for viscous transport. Thus, our results suggest that upon variation of the RTIL's anion, the rotational dynamics of dicyanamide is largely determined by dicyanamide−cation interactions. Conversely, the different structure and dynamics of the studied RTILs have only a minor impact on the rotational dynamics of the dicyanamide anion. Hence, upon substitution of the RTIL's anions, the vibrational probe dicyanamide rather investigates local interactions and dynamics. As such, the observed dynamics is rather specific to the used anionic probe molecule and its local environment.

ASSOCIATED CONTENT

Supporting Information

The Supporting Information is available free of charge on the ACS Publications website at DOI: 10.1021/acs.jpcb.8b10849.

Infrared absorption spectra of [emim][DCA] and $[emim][BF_4]$; state spectra using a parallel relaxation model; vibrational relaxation times of $[DCA]^-$ in $[emim][EtSO_4]$, $[emim][NTf_2]$, and [emim][OTf]; correlation between slow vibrational relaxation and viscosity; $R(t)$ decays for $[DCA]^-$ in $[emim][EtSO_4]$, $[emim][NTf_2]$, and [emim][OTf]; correlation between rotation times and viscosity (PDF)

AUTHOR INFORMATION

Corresponding Author

*E-mail: hunger@mpip-mainz.mpg.de. Phone: +49-6131-379-765. Fax: +49-6131-379-360.

DOI: 10.1021/acs.jpcb.8b10849
J. Phys. Chem. B XXXX, XXX, XXX−XXX

ORCID

Johannes Hunger: 0000-0002-4419-5220
Maksim Grechko: 0000-0002-7717-387X
Mischa Bonn: 0000-0001-6851-8453

Notes

The authors declare no competing financial interest.

■ ACKNOWLEDGMENTS

S.R. is a recipient of a DFG fellowship/DFG-funded position through the Excellence Initiative by the Graduate School Materials Science in Mainz (GSC 266). J.H. acknowledges the funding from the European Research Council (ERC) under the European Union's Horizon 2020 research and innovation programme (grant agreement no. 714691).

■ REFERENCES

(1) Rumble, C. A.; Uitvlugt, C.; Conway, B.; Maroncelli, M. Solute Rotation in Ionic Liquids: Size, Shape, and Electrostatic Effects. *J. Phys. Chem. B* **2017**, *121*, 5094−5109.
(2) Castner, E. W.; Wishart, J. F.; Shirota, H. Intermolecular Dynamics, Interactions, and Solvation in Ionic Liquids. *Acc. Chem. Res.* **2007**, *40*, 1217−1227.
(3) Hayes, R.; Warr, G. G.; Atkin, R. Structure and Nanostructure in Ionic Liquids. *Chem. Rev.* **2015**, *115*, 6357−6426.
(4) Dommert, F.; Wendler, K.; Berger, R.; Delle Site, L.; Holm, C. Force Fields for Studying the Structure and Dynamics of Ionic Liquids: A Critical Review of Recent Developments. *ChemPhysChem* **2012**, *13*, 1625−1637.
(5) Samanta, A. Solvation Dynamics in Ionic Liquids: What We Have Learned from the Dynamic Fluorescence Stokes Shift Studies. *J. Phys. Chem. Lett.* **2010**, *1*, 1557−1562.
(6) Fruchey, K.; Fayer, M. D. Dynamics in Organic Ionic Liquids in Distinct Regions Using Charged and Uncharged Orientational Relaxation Probes. *J. Phys. Chem. B* **2010**, *114*, 2840−2845.
(7) Castner, E. W.; Wishart, J. F. Spotlight on Ionic Liquids. *J. Chem. Phys.* **2010**, *132*, No. 120901.
(8) Brinzer, T.; Garrett-Roe, S. Temperature and Chain Length Dependence of Ultrafast Vibrational Dynamics of Thiocyanate in Alkylimidazolium Ionic Liquids: A Random Walk on a Rugged Energy Landscape. *J. Chem. Phys.* **2017**, *147*, No. 194501.
(9) Hunger, J.; Buchner, R. *Dielectric Properties of Ionic Liquids*; Paluch, M., Ed.; Springer International Publishing: Cham, 2016; pp 53−71.
(10) Araque, J. C.; Hettige, J. J.; Margulis, C. J. Modern Room Temperature Ionic Liquids, a Simple Guide to Understanding Their Structure and How It May Relate to Dynamics. *J. Phys. Chem. B* **2015**, *119*, 12727−12740.
(11) Hu, Z.; Margulis, C. J. Heterogeneity in a Room-Temperature Ionic Liquid: Persistent Local Environments and the Red-Edge Effect. *Proc. Natl. Acad. Sci. U.S.A.* **2006**, *103*, 831−836.
(12) Hallett, J. P.; Welton, T. Room-Temperature Ionic Liquids: Solvents for Synthesis and Catalysis. 2. *Chem. Rev.* **2011**, *111*, 3508−3576.
(13) Sonnleitner, T.; Turton, D. A.; Hefter, G.; Ortner, A.; Waselikowski, S.; Walther, M.; Wynne, K.; Buchner, R. Ultra-Broadband Dielectric and Optical Kerr-Effect Study of the Ionic Liquids Ethyl and Propylammonium Nitrate. *J. Phys. Chem. B* **2015**, *119*, 8826−8841.
(14) Hunger, J.; Sonnleitner, T.; Liu, L.; Buchner, R.; Bonn, M.; Bakker, H. J. Hydrogen-Bond Dynamics in a Protic Ionic Liquid: Evidence of Large-Angle Jumps. *J. Phys. Chem. Lett.* **2012**, *3*, 3034−3038.
(15) Zheng, Z.-P.; Fan, W.; Roy, S.; Mazur, K.; Nazet, A.; Buchner, R.; Bonn, M.; Hunger, J. Ionic Liquids: Not Only Structurally but Also Dynamically Heterogeneous. *Angew. Chem., Int. Ed.* **2015**, *54*, 687−690.
(16) Yamada, S. A.; Bailey, H. E.; Tamimi, A.; Li, C.; Fayer, M. D. Dynamics in a Room-Temperature Ionic Liquid from the Cation Perspective: 2D IR Vibrational Echo Spectroscopy. *J. Am. Chem. Soc.* **2017**, *139*, 2408−2420.
(17) Zhang, X.-X.; Breffke, J.; Ernsting, N. P.; Maroncelli, M. Observations of Probe Dependence of the Solvation Dynamics in Ionic Liquids. *Phys. Chem. Chem. Phys.* **2015**, *17*, 12949−12956.
(18) Wishart, J. Importance of Ionic Liquid Solvation Dynamics to Their Applications in Advanced Devices and Systems. *J. Phys. Chem. Lett.* **2010**, *1*, 1629−1630.
(19) Lawler, C.; Fayer, M. D. The Influence of Lithium Cations on Dynamics and Structure of Room Temperature Ionic Liquids. *J. Phys. Chem. B* **2013**, *117*, 9768−9774.
(20) Zhang, X.; Liang, M.; Hunger, J.; Buchner, R.; Maroncelli, M. Dielectric Relaxation and Solvation Dynamics in a Prototypical Ionic Liquid + Dipolar Protic Liquid Mixture: 1-Butyl-3-Methylimidazolium Tetrafluoroborate + Water. *J. Phys. Chem. B* **2013**, *117*, 15356−15368.
(21) Lang, B.; Angulo, G.; Vauthey, E. Ultrafast Solvation Dynamics of Coumarin 153 in Imidazolium-Based Ionic Liquids. *J. Phys. Chem. A* **2006**, *110*, 7028−7034.
(22) Ito, N.; Arzhantsev, S.; Maroncelli, M. The Probe Dependence of Solvation Dynamics and Rotation in the Ionic Liquid 1-Butyl-3-Methyl-Imidazolium Hexafluorophosphate. *Chem. Phys. Lett.* **2004**, *396*, 83−91.
(23) Giammanco, C. H.; Kramer, P. L.; Wong, D. B.; Fayer, M. D. Water Dynamics in 1-Alkyl-3-Methylimidazolium Tetrafluoroborate Ionic Liquids. *J. Phys. Chem. B* **2016**, *120*, 11523−11538.
(24) Giammanco, C. H.; Kramer, P. L.; Yamada, S. A.; Nishida, J.; Tamimi, A.; Fayer, M. D. Coupling of Carbon Dioxide Stretch and Bend Vibrations Reveals Thermal Population Dynamics in an Ionic Liquid. *J. Phys. Chem. B* **2016**, *120*, 549−556.
(25) Sando, G. M.; Dahl, K.; Owrutsky, J. C. Vibrational Spectroscopy and Dynamics of Azide Ion in Ionic Liquid and Dimethyl Sulfoxide Water Mixtures. *J. Phys. Chem. B* **2007**, *111*, 4901−4909.
(26) Owrutsky, J.; Houchins, C.; Weidinger, D.; Brown, D. Vibrational Spectra and Dynamics of Anions and Acids in Ionic Liquids. *ECS Trans.* **2010**, *33*, 621−626.
(27) Dahl, K.; Sando, G. M.; Fox, D. M.; Sutto, T. E.; Owrutsky, J. C. Vibrational Spectroscopy and Dynamics of Small Anions in Ionic Liquid Solutions. *J. Chem. Phys.* **2005**, *123*, No. 084504.
(28) Ren, Z.; Brinzer, T.; Dutta, S.; Garrett-Roe, S. Thiocyanate as a Local Probe of Ultrafast Structure and Dynamics in Imidazolium-Based Ionic Liquids: Water-Induced Heterogeneity and Cation-Induced Ion Pairing. *J. Phys. Chem. B* **2015**, *119*, 4699−4712.
(29) Dutta, S.; Ren, Z.; Brinzer, T.; Garrett-Roe, S. Two-Dimensional Ultrafast Vibrational Spectroscopy of Azides in Ionic Liquids Reveals Solute-Specific Solvation. *Phys. Chem. Chem. Phys.* **2015**, *17*, 26575−26579.
(30) Ren, Z.; Ivanova, A. S.; Couchot-Vore, D.; Garrett-Roe, S. Ultrafast Structure and Dynamics in Ionic Liquids: 2D-IR Spectroscopy Probes the Molecular Origin of Viscosity. *J. Phys. Chem. Lett.* **2014**, *5*, 1541−1546.
(31) Kim, H.; Cho, M. Infrared Probes for Studying the Structure and Dynamics of Biomolecules. *Chem. Rev.* **2013**, *113*, 5817−5847.
(32) Tamimi, A.; Bailey, H. E.; Fayer, M. D. Alkyl Chain Length Dependence of the Dynamics and Structure in the Ionic Regions of Room-Temperature Ionic Liquids. *J. Phys. Chem. B* **2016**, *120*, 7488−7501.
(33) Tamimi, A.; Fayer, M. D. Ionic Liquid Dynamics Measured with 2D IR and IR Pump-Probe Experiments on a Linear Anion and the Influence of Potassium Cations. *J. Phys. Chem. B* **2016**, *120*, 5842−5854.
(34) Yoshida, Y.; Baba, O.; Saito, G. Ionic Liquids Based on Dicyanamide Anion: Influence of Structural Variations in Cationic Structures on Ionic Conductivity. *J. Phys. Chem. B* **2007**, *111*, 4742−4749.

DOI: 10.1021/acs.jpcb.8b10849
J. Phys. Chem. B XXXX, XXX, XXX−XXX

(35) Tan, H.-S.; Piletic, I. R.; Fayer, M. D. Polarization Selective Spectroscopy Experiments: Methodology and Pitfalls. *J. Opt. Soc. Am. B* **2005**, *22*, 2009.
(36) Mazur, K.; Bonn, M.; Hunger, J. Hydrogen Bond Dynamics in Primary Alcohols: A Femtosecond Infrared Study. *J. Phys. Chem. B* **2015**, *119*, 1558−1566.
(37) Tros, M.; Woutersen, S. Polarization-Modulation Setup for Ultrafast Infrared Anisotropy Experiments to Study Liquid Dynamics. *Opt. Lett.* **2015**, *40*, 2607−2609.
(38) Hunger, J.; Tielrooij, K. J.; Buchner, R.; Bonn, M.; Bakker, H. J. Complex Formation in Aqueous Trimethylamine-N-Oxide (TMAO) Solutions. *J. Phys. Chem. B* **2012**, *116*, 4783−4795.
(39) Chuntonov, L.; Kuroda, D. G.; Ghosh, A.; Ma, J.; Hochstrasser, R. M. Quantum Beats and Coherence Decay in Degenerate States Split by Solvation. *J. Phys. Chem. Lett.* **2013**, *4*, 1866−1871.
(40) Pakoulev, A. V.; Rickard, M. A.; Mathew, N. A.; Kornau, K. M.; Wright, J. C. Frequency-Domain Time-Resolved Four Wave Mixing Spectroscopy of Vibrational Coherence Transfer with Single-Color Excitation. *J. Phys. Chem. A* **2008**, *112*, 6320−6329.
(41) Schreiner, C.; Zugmann, S.; Hartl, R.; Gores, H. J. Temperature Dependence of Viscosity and Specific Conductivity of Fluoroborate-Based Ionic Liquids in Light of the Fractional Walden Rule and Angell's Fragility Concept. *J. Chem. Eng. Data* **2010**, *55*, 4372−4377.
(42) Gaciño, F. M.; Regueira, T.; Lugo, L.; Comuñas, M. J. P.; Fernández, J. Influence of Molecular Structure on Densities and Viscosities of Several Ionic Liquids. *J. Chem. Eng. Data* **2011**, *56*, 4984−4999.
(43) Schreiner, C.; Zugmann, S.; Hartl, R.; Gores, H. J. Fractional Walden Rule for Ionic Liquids: Examples from Recent Measurements and a Critique of the So-Called Ideal KCl Line for the Walden Plot †. *J. Chem. Eng. Data* **2010**, *55*, 1784−1788.
(44) Harris, K. R.; Kanakubo, M. Self-Diffusion Coefficients and Related Transport Properties for a Number of Fragile Ionic Liquids. *J. Chem. Eng. Data* **2016**, *61*, 2399−2411.
(45) Piatkowski, L.; Eisenthal, K. B.; Bakker, H. J. Ultrafast Intermolecular Energy Transfer in Heavy Water. *Phys. Chem. Chem. Phys.* **2009**, *11*, 9033−9038.
(46) Woutersen, S.; Bakker, H. J. Resonant Intermolecular Transfer of Vibrational Energy in Liquid Water. *Nature* **1999**, *402*, 507−509.
(47) Liu, L.; Hunger, J.; Bakker, H. J. Energy Relaxation Dynamics of the Hydration Complex of Hydroxide. *J. Phys. Chem. A* **2011**, *115*, 14593−14598.
(48) Stoppa, A.; Buchner, R.; Hefter, G. How Ideal Are Binary Mixtures of Room-Temperature Ionic Liquids? *J. Mol. Liq.* **2010**, *153*, 46−51.
(49) Giammanco, C. H.; Yamada, S. A.; Kramer, P. L.; Tamimi, A.; Fayer, M. D. Structural and Rotational Dynamics of Carbon Dioxide in 1-Alkyl-3-Methylimidazolium Bis(Trifluoromethylsulfonyl)Imide Ionic Liquids: The Effect of Chain Length. *J. Phys. Chem. B* **2016**, *120*, 6698−6711.

DOI: 10.1021/acs.jpcb.8b10849
J. Phys. Chem. B XXXX, XXX, XXX−XXX